# Coordination geometrical effect on LMCT-depended energy transfer processes of luminescent Eu(III) complexes

*Pedro Paulo Ferreira da Rosa,[a] Shiori Miyazaki,[e] Haruna Sakamoto,[e] Yuichi Kitagawa,[b,d] Kiyoshi Miyata,[e] Tomoko Akama,[c] Masato Kobayashi,[c,d] Koji Fushimi,[b] Ken Onda,[e] Tetsuya Taketsugu,[c,d] and Yasuchika Hasegawa[b,d*]*

[a]Graduate School of Chemical Sciences and Engineering, Hokkaido University, Sapporo, 060-8628, Japan.

[b]Faculty of Engineering, Hokkaido University, Sapporo, 060-8628, Japan.

[c]Faculty of Science, Hokkaido University, Sapporo, 060-0810, Japan.

[d]Institute for Chemical Reaction Design and Discovery (WPI-ICReDD), Hokkaido University, Sapporo, 001-0021, Japan.

[e]Department of Chemistry, Kyushu University, Fukuoka 829-0395, Japan

Email: hasegaway@eng.hokudai.ac.jp

Keywords: Coordination geometry, LMCT, Europium, Luminescence, β-diketonate

## Abstract

Photophysical properties of europium (Eu(III)) complexes are affected by ligand-to-metal charge transfer (LMCT) states. Two luminescent Eu(III) complexes with three tetramethylheptadionates (tmh) and pyridine (py), $[Eu(tmh)_3(py)_1]$ (seven-coordinated monocapped-octahedral structure) and $[Eu(tmh)_3(py)_2]$ (eight-coordinated square anti-prismatic structure), were synthesized for geometrical-induced LMCT level control. Distances between Eu(III) and oxygen atoms of tmh ligands were estimated using single-crystal X-ray analyses. The contribution percentages of π-4*f* mixing in HOMO and LUMO at the optimized-structure in the ground state were calculated using DFT (LC-BLYP). The Eu-O distances and their π-4*f* mixed orbitals affect the energy level of LMCT states in Eu(III) complexes. The LMCT energy level of eight-coordinated Eu(III) complex was higher than that of seven-coordinated Eu(III) complex. The energy transfer processes between LMCT and Eu(III) ion were investigated using temperature-dependent and time-resolved emission lifetime measurements of $^5D_0 \rightarrow {}^7F_J$ transitions of Eu(III) ions. In this study, the LMCT-dependent energy transfer processes of seven- and eight-coordinated Eu(III) complexes are demonstrated for the first time.

## Introduction

Luminescent metal complexes have been studied because of their versatile photophysical properties for applications such as optical materials,[1–8] light-emitting diodes,[9] cellular probes and sensors.[10–15] Their photophysical properties are strongly affected by coordination structure, coordination number, and organic ligand moieties. Many types of luminescent metal complexes with metal-to-ligand charge transfer (MLCT), metal-metal to ligand charge transfer (MMCLT) and ligand-to-metal charge transfer (LMCT) bands have been reported.[16] In particular, there have been a number of studies on the control of the MLCT emission processes of Ir(III) and

Ru(II) complexes.[17,18] Recently, the control of the LMCT transition in Fe(II) complexes has also been described.[19] The charge-transfer bands are directly related to the electronic and geometrical structures of the metal complex.

The electronic transitions of luminescent lanthanide complexes are significantly different from those of transition metal complexes. Lanthanide complexes show characteristic photophysical properties derived from the metal-centered 4*f*-4*f* transitions. The 4*f*-4*f* emission is based on the electric-dipole transition with small offset (non-Stokes shifts)[20], which leads to distinctive emission with high color purity (fwhm < 10 nm) and long emission lifetime (>1 μs).[21] Since the 4*f*-4*f* electric-dipole transitions in lanthanide complexes are Laporte-forbidden, a mixed-parity state and field perturbations in 4*f* orbitals are required to partially allow the 4*f*-4*f* transition.[22,23] The charge-transfer bands in europium (Eu(III)) complexes have been also reported.[24] In this study, we focus on the 4*f*-4*f* emission process of Eu(III) complexes depending on the LMCT bands.

The LMCT bands of Eu(III) complexes with organic anion ligands such as acetylacetonate (acac)[25], trimethylheptanoate (tmh)[26–29], polycyclic aromatic hydrocarbons[30,31] and dialkyldithiocarbamates[32,33] have been reported. Faustino reported a theoretical approach for understanding the influence of LMCT bands in lanthanide compounds and found that the energy levels of triplet and LMCT bands are important for efficient europium ion sensitization.[34] Experimentally, the LMCT at low-lying energy level have been largely reported as a quenching site for Eu(III)-based luminescence.[35,36] Miranda showed that effective distortion and strain in tmh ligand of a di-nuclear Eu(III) complex promotes change in the energy level of the LMCT states.[28] The hybridized orbital between the non-bonding electron of organic ligand and *f* orbital of lanthanide ion has also been reported.[37] We have recently reported on a series of seven-coordinated Eu(III) complexes using tmh and phosphine oxide ligands with several polyhedral structures around the Eu(III) ion.[38] The radiative rate constant

of the Eu(III) complex with a monocapped-octahedral structure (Point group: $C_{3v}$) was larger than those of Eu(III) complex with monocapped-trigonal-prismatic (Point group: $C_{2v}$) and pentagonal-bipyramidal structures (Point group: $D_{5h}$) because of larger mixing of LMCT states into the 4*f* states. Coordination polyhedral structure directly affects the electron density and the distance between coordinating atoms and lanthanide ion, resulting in changes of the LMCT states in the Eu(III) complex. The theoretical and experimental investigation of photophysical relationship between geometrical structure and LMCT energy level leads to a well-understanding of LMCT-dependent energy transfer process in Eu(III) complexes.

In order to analyze the energy transfer process related to the LMCT state, we prepared seven- and eight-coordinated Eu(III) complexes using tmh and pyridine (py) ligands, [Eu(tmh)$_3$(py)$_1$] (Eu-py1) and [Eu(tmh)$_3$(py)$_2$] (Eu-py2) (Figure 1). Their coordination structures were characterized using single-crystal X-ray analyses. The photophysical processes of the Eu(III) complexes were evaluated using diffuse reflectance spectra, emission spectra, lifetimes and quantum yields. The quantum chemical calculations were performed to provide insights into the LMCT states in seven- and eight-coordinated structures. The LMCT energy level of eight-coordinated Eu(III) complex was higher than that of seven-coordinated Eu(III) complex. The temperature-dependent and time-resolved emission lifetimes were also recorded to understand the characteristic energy transfer pathways related to the LMCT state of each Eu(III) complex. In this study, the LMCT-controlled energy transfer processes for photosensitized luminescence of seven- and eight-coordinated Eu(III) complexes are demonstrated.

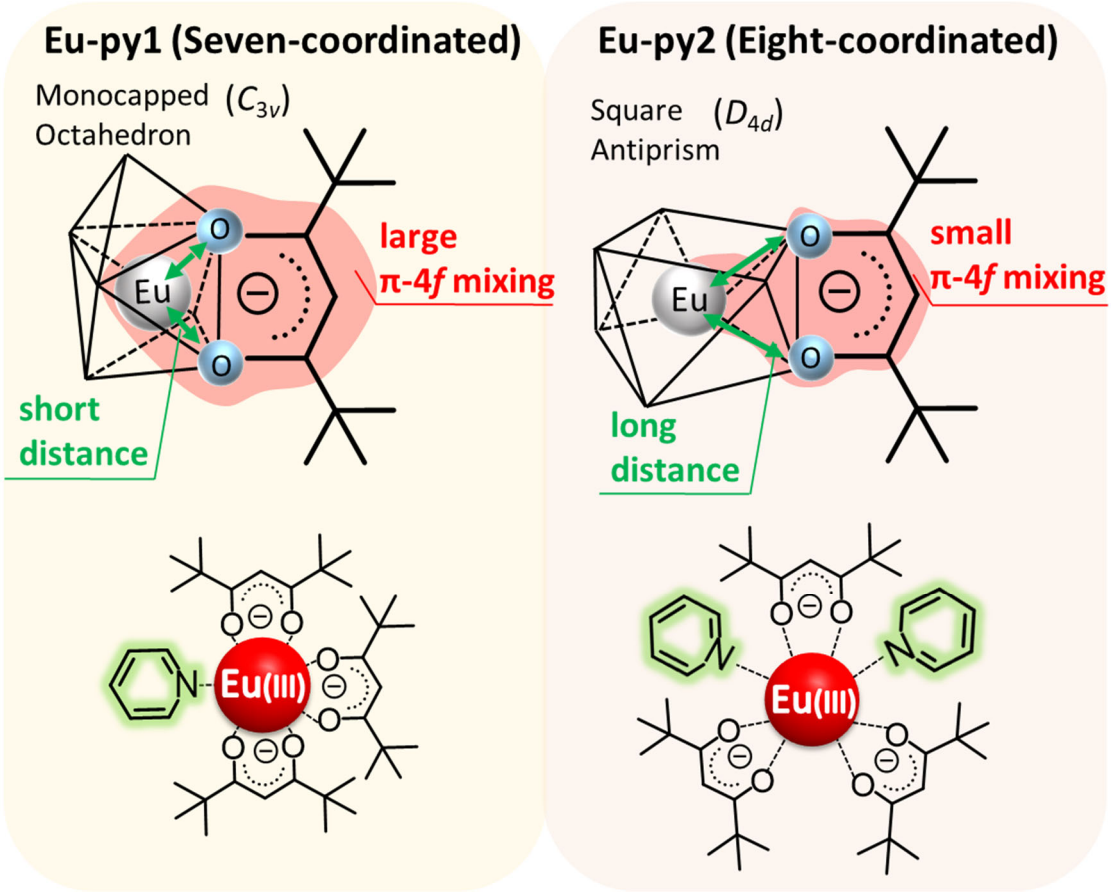


**Figure 1.** Effect of coordination geometrical structures in the distance and orbital mixing of coordinating ligands and Eu(III) ion.

## Experimental Section

**General Methods.** All chemicals were reagent grade and used without further purification. Infrared spectra were recorded on a JASCO FT/IR-4200 spectrometer. Elemental analyses were performed on a J-Science Lab JM 10 Micro Corder and an Exeter Analytical CE440. Mass spectrometry (ESI-MS) were recorded on a JEOL JMS-T100LP.

**Preparation of [Eu(tmh)$_3$(py)$_1$] (Eu-py1) and [Gd(tmh)$_3$(py)$_1$] (Gd-py1).** The precursor complex, [Eu$_2$(tmh)$_6$], was synthesized as described in the previous report.[39] Eu-py1 synthesis was based on the previous report[40] of the same compound with minor adaptations. [Eu$_2$(tmh)$_6$] (0.17 g, 0.120 mmol) and pyridine (0.04 g, 0.5 mmol) were dissolved in methanol. The solution was heated at reflux while stirring for 3 h. The solution was evaporated and the obtained solid

was washed with distilled water and dichloromethane. Then, they were recrystallized in methanol giving yellowish crystals for Eu-py1.

**Eu-py1**: Yield: 0.12 g (70%). IR (ATR) $\nu$ = 2830-3003 (m, C-H), 1569 (s, C=O) $cm^{-1}$. Elemental analysis calc.(%) for [$C_{38}H_{62}NO_6Eu$] + 0.5 $CH_2Cl_2$ + 0.5 $H_2O$: C, 55.56; H, 7.75; N, 1.68. Found C, 55.58; H, 7.73; N, 1.67.

Gd-py1 was synthesized with the same method as Eu-py1. Recrystallized crystals were transparent for Gd-py1.

**Gd-py1**: Yield: 0.12 g (70%). IR (ATR) $\nu$ = 2830-3003 (m, C-H), 1569 (s, C=O) $cm^{-1}$. Elemental analysis calc.(%) for [$C_{38}H_{62}NO_6Gd$]: C, 58.06; H, 7.95; N, 1.78. Found C, 57.88; H, 7.97; N, 1.75.

**Preparation of [Eu(tmh)$_3$(py)$_2$] (Eu-py2) and [Gd(tmh)$_3$(py)$_2$] (Gd-py2).** Eu-py2 synthesis was based on the previous report[41] of the same compound with minor adaptations. [$Eu_2(tmh)_6$] (0.17 g, 0.120 mmol) was dissolved directly into pyridine and the solution was heated at reflux while stirring for 30 min. The solution was evaporated and the obtained solid was washed with distilled water and dichloromethane. Then, they were recrystallized in pyridine giving slight yellow crystals for Eu-py2. These compounds were not stable under temperatures higher than 30 $^{o}$C, so proper storage is recommended (refrigerator or under pyridine gas storage).

**Eu-py2**: Yield: 0.07 g (40%). IR (ATR) $\nu$ = 2831-3006 (m, C-H), 1569 (s, C=O) $cm^{-1}$. Elemental analysis calc.(%) for [$C_{43}H_{67}N_2O_6Eu$] + 0.2 $CH_2Cl_2$: C, 59.17; H, 7.75; N, 3.19. Found C, 59.22; H, 7.82; N, 3.05.

Gd-py2 was synthesized with the same method as Eu-py2. Recrystallized crystals were transparent for Gd-py2.

**Gd-py2**: Yield: 0.12 g (70%). IR (ATR) $\nu$ = 2831-3006 (m, C-H), 1569 (s, C=O) $cm^{-1}$. Elemental analysis calc.(%) for [$C_{43}H_{67}N_2O_6Gd$] + 0.25 $CH_2Cl_2$: C, 58.60; H, 7.68; N, 3.16. Found C, 58.61; H, 7.75; N, 3.02.

**Optical Measurements.** Diffuse reflection spectra were obtained using a JASCO V-670 spectrophotometer with an ISN-723 integrating-sphere unit. Emission and excitation spectra were recorded on a HORIBA Fluorolog-3 spectrofluorometer and corrected for the response of the detector system. Emission lifetimes ($\tau_{obs}$) were measured using the third harmonics (355 nm) of a Q-switched Nd:YAG laser (Spectra Physics, INDI-50, fwhm = 5 ns, $\lambda$ = 1064 nm) and a photomultiplier (Hamamatsu Photonics, R5108, response time ≤ 1.1 ns). The Nd:YAG laser response was monitored with a digital oscilloscope (Sony Tektronix, TDS3052, $f$ = 500 MHz) synchronized to the single-pulse excitation. Emission lifetimes were determined from the slope of logarithmic plots of the decay profiles. The emission quantum yields excited at 330 ($\Phi_{\pi\text{-}\pi^*}$), 400 ($\Phi_{LMCT}$), 464 ($\Phi_{ff}$) and 530 nm ($\Phi_{ff}$) were estimated using a JASCO F-6300-H spectrometer attached with a JASCO ILF-533 integrating sphere unit ($\varphi$ = 100 nm) under air and argon. The wavelength dependence of the detector response and the beam intensity of the Xe light source for each spectrum were calibrated using a standard light source.

Detection of time-resolved photoluminescence measurements were performed using a streak camera (Hamamatsu C4334) coupled to a polychromator (SpectraPro-150, spectral resolution: ≃ 10 nm, Acton Research Corporation). The detection system was synchronized to a regenerative Ti:Sapphire amplifier (Spitfire Ace, ~120 fs, 1 kHz, 4 mJ/pulse, 800 nm, Spectra Physics) or an optical parametric oscillator (OPO) system (EKSPLA NT220, central wavelength : tunable 400 - 2000 nm, pulse duration: 3 ns). The samples were pumped by the second harmonic generation (SHG; 400 nm), or third harmonic generation (THG; 267 nm) of a fundamental pulse from the amplifier, or the output from the OPO (465 nm). The polarization angles of the light for pumping and detection were set to the magic angle (54.7 deg) to avoid

distortion of the temporal profiles from molecular orientation.[42] Emission lifetimes in the range of 250-325 K were measured using a cryostat (Thermal Block Company, SA-SB245T) and a temperature controller (Oxford Instruments, ITC 502S).

Seven-coordinated Eu-py1 was unstable at many solvent conditions (ex: methanol, acetone, dichloromethane), where pyridine ligand is easily dissociated. For Eu-py2, the complex dissolved in pyridine itself showed good stability. Therefore, in this paper, we focused on the crystal samples of Eu-py1 and Eu-py2 only.

**Crystallography.** The X-ray crystal structures and crystallographic data for Ln-py1 and Ln-py2 are shown in Figure 2 and Table S1 (see supporting information). Identical structures of Eu(III) and Gd(III) complexes were obtained. All measurements were made on a Rigaku XtaLAB PRO MM007 imaging plate area detector with graphite monochromatic Mo-$K_\alpha$ radiation. Corrections for decay and Lorentz-polarization effects were made using empirical absorption correction, solved by direct methods and expanded using Fourier techniques. Non-hydrogen atoms were refined anisotropically using the SHELX system.[43] Hydrogen atoms were refined using the riding model. All calculations were performed using the crystal structure crystallographic and Olex 2 software package.[44] The CIF data was confirmed by the checkCIF/PLATON service. CCDC-1979576 (for Eu-py1), CCDC-1979572 (for Eu-py2), CCDC-1979575 (for Gd-py1), CCDC-1979571 (for Gd-py2) contain the supplementary crystallographic data for this paper. These data can be obtained free of charge from The Cambridge Crystallographic Data Centre via www.ccdc.cam.ac.uk/data_request/cif.

**Computational Details.** Quantum chemical calculations were performed by the density functional theory (DFT) using the *Gaussian 16* package.[45] Geometry optimization was carried out using DFT with B3LYP-D3 functional,[46–48] while excited states were investigated using time-depended (TD) DFT with the long-range corrected (LC) BLYP functional.[49–51] The Grimme's D3 dispersion correction is incorporated since the intramolecular dispersion

interaction plays significant role for the stabilization of these systems including many aromatic rings. The cc-pVDZ basis set[52] was used for all elements, except for Eu(III), in which Stuttgart RECP (ECP28MWB) basis set was used.[53]

# Results

## Structure

Seven-coordinated (CN-7) and eight-coordinated (CN-8) Eu(III) complexes with tmh and py ligands were independently synthesized using different methods. $[Eu(tmh)_3(py)_1]$ (Eu-py1) was synthesized by the complexation of pyridine (4 eq) with precursor $[Eu_2(tmh)_6]$ in methanol for 3h (SI: Scheme S1). On the other hand, $[Eu(tmh)_3(py)_2]$ (Eu-py2) was prepared by the complexation of precursor $[Eu_2(tmh)_6]$ in pyridine solvent for 30 min (SI: Scheme S1). The single crystals of Eu-py1 and Eu-py2 were obtained by recrystallization from methanol and pyridine solutions, respectively. The structures of Eu-py1 and Eu-py2 were analyzed using X-ray single-crystal measurements (Figure 2a and Figure 2b). The Eu-py1 is composed of three tmh and one pyridine ligands, forming a seven-coordinated structure. For Eu-py2, two pyridines are coordinated to an $Eu(tmh)_3$ unit, resulting in the formation of an eight-coordinated structure.[54]

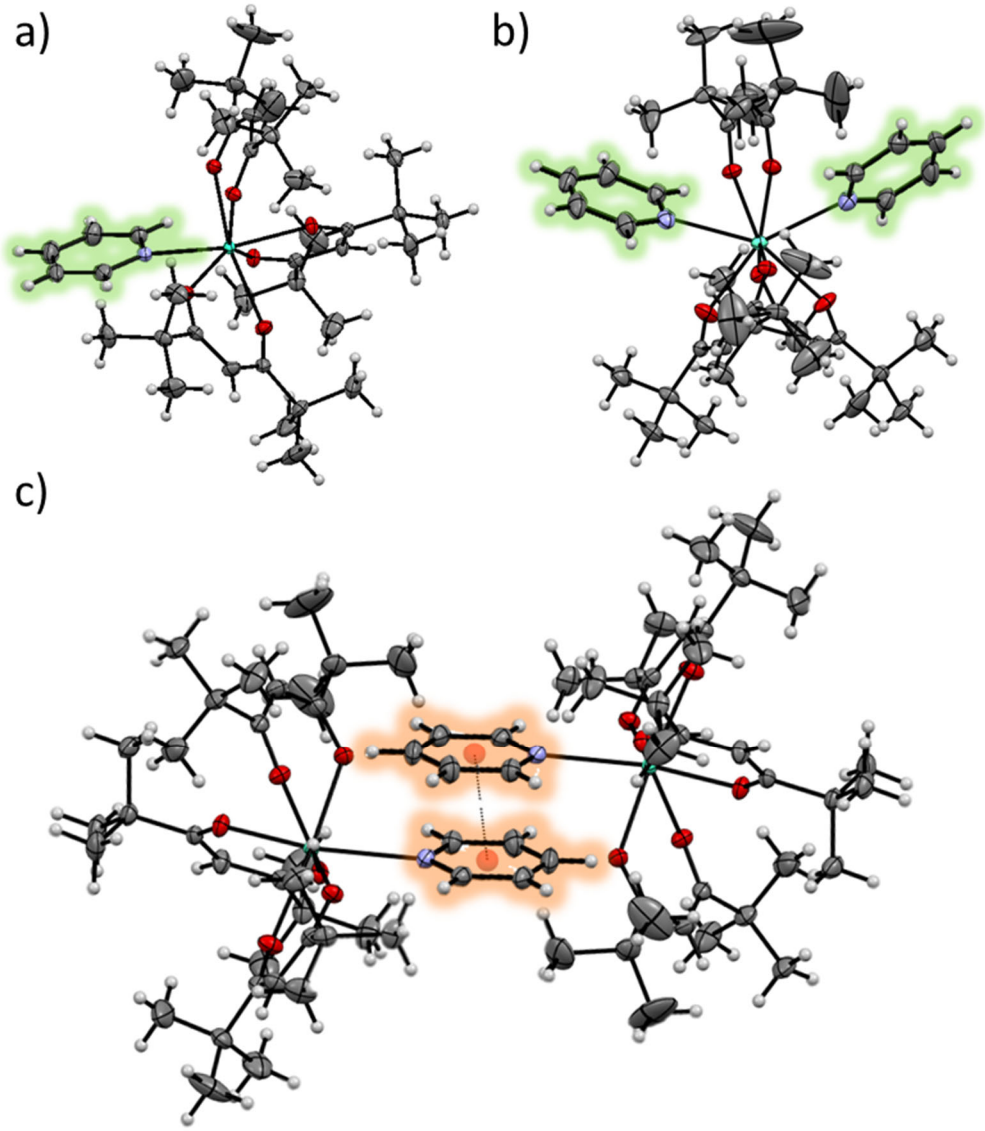


**Figure 2.** View of a) Ln-py1 (CN-7) and b) Ln-py2 (CN-8) showing 50% probability displacement ellipsoids. c) π/π interactions in Ln-py1 crystal structure. Pyridine ligands glowing for emphasis.

The bidentate β-diketonate ligands present average Eu-$O_{tmh}$ distances of 2.296 Å for Eu-py1 and 2.325 Å for Eu-py2, respectively. The minimum and maximum Eu-$O_{tmh}$ distances were also found to be 2.252 Å and 2.314 Å for Eu-py1, 2.286 Å and 2.347 Å for Eu-py2, respectively. Pyridine ligands show average Eu-N distances of 2.538 Å for Eu-py1 and 2.601 Å for Eu-py2 (Eu-N1: 2.598 Å, Eu-N2: 2.603 Å). The distances for Eu-py2 (CN-8) between coordinated

atoms and Eu(III) ion are larger than those for Eu-py1 (CN-7). We also observed specific intermolecular CH/π and π/π interactions in the Eu-py1 structure (Figure 2c). These specific interactions can stabilize the characteristic CN-7 structure. The degree of planarity deviation of tmh ligands in Eu-py1 is similar to that of Eu-py2.[55] The structures of Gd-py1 and Gd-py2 are isostructural with the corresponding Eu-py1 and Eu-py2, respectively (SI: Table S1).

Based on the crystal structures, we performed continuous shape measures (CShM) calculations using SHAPE[56–58] to determine the coordination geometrical structures around the Eu(III) ions in the first coordination sphere. The $S_{\mathrm{CShM}}$ criterion represents the degree of deviation from ideal coordination structure, and is given by the following equation:

$$S_{\mathrm{CShM}} = \min \frac{\Sigma_k^N |Q_k - P_k|^2}{\Sigma_k^N |Q_k - Q_0|^2} \times 100 \qquad (1),$$

where $Q_k$ is the vertices of an actual structure, $Q_0$ is the center of mass of an actual structure, $P_k$ is the vertices of an ideal structure, and $N$ is the number of vertices. The estimated $S_{\mathrm{CShM}}$ values of the Eu(III) complexes are summarized in Table S2 and Table S3 (see supporting information). Based on the minimum value of $S_{\mathrm{CShM}}$, the pseudo-coordination polyhedral structures of Eu-py1 and Eu-py2 were categorized to be 7-MCO (monocapped-octahedron, point group: $C_{3v}$) and 8-SAP (Square antiprism, point group: $D_{4d}$), respectively. The coordination geometry of Eu-py1 (CN-7) is more asymmetric than that of Eu-py2 (CN-8). According to the crystal-field perturbation theories,[22,23] Eu-py1 is expected to show larger radiative rate constant $k_r$.

## Absorption, excitation and emission properties

The energy level of LMCT influences the energy transfer processes of Eu(III) complexes directly. The low-lying LMCT bands (close to Eu(III) excited states) can work as quenching sites for the Eu(III)-based luminescence.[35,36] In order to observe the LMCT bands in Eu(III) complexes, the diffuse reflection spectra were measured (Figure 3). For the estimation of LMCT bands, the spectra for Gd-py1 and Gd-py2 were also shown in Figure 3.[59] The

absorption bands at 320 nm (31250 $cm^{-1}$) for Eu-py1 and Eu-py2 were assigned to singlet π–π* and/or σ–π* transitions of the tmh ligands, which agree with the absorption spectra of Gd-py1 and Gd-py2. We also observed absorption bands at around 370 nm (27,000 $cm^{-1}$) for the Eu(III) complexes. The absorption bands at 370 nm for Gd(III) complexes were not observed. Considering the absorption spectra of the Eu(III) and Gd(III) complexes, the absorption band at around 370 nm is contributed to the LMCT transition. The absorption in LMCT band in Eu-py1 is slightly red-shifted compared to Eu-py2 (SI: Figure S3). Their absorption bands were assigned to $^{7}$LMCT transitions by using TD-DFT calculations (Table 3 and Table 4). These findings suggest that shorter Eu-$O_{tmh}$ distance in Eu-py1 (CN-7) provides stronger electronic interactions between the β-diketonate ligands and Eu(III) center, resulting in formation of lower LMCT energy level.

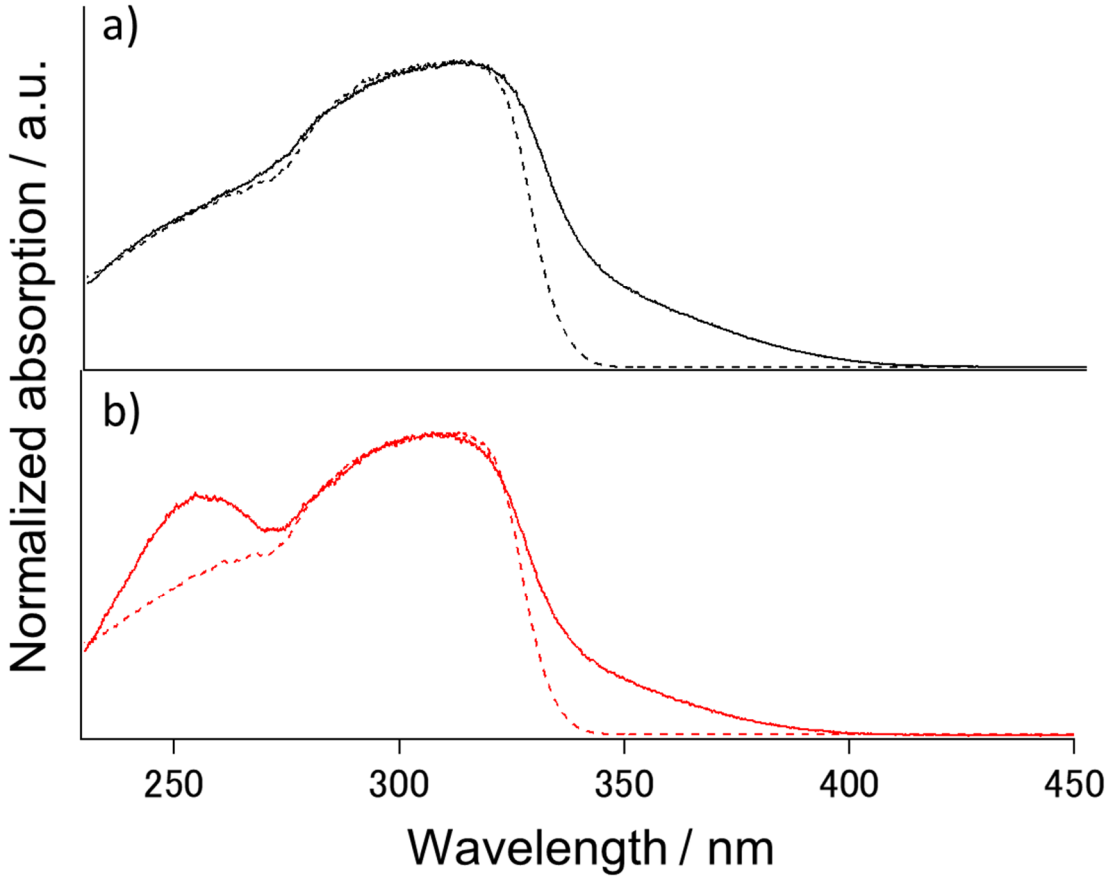

**Figure 3.** Diffuse reflection spectra of Eu-py1 (a: black line) and Gd-py1 (a: black dash line) on the top, Eu-py2 (b: red line) and Gd-py2 (b: red dash line) on the bottom.

Excitation and emission spectra of Eu-py1 and Eu-py2 in solids are shown in Figure 4. They were normalized concerning their maximum peaks.[60] Distinguishable 4*f* intra-configurational excitation bands, $^7F_J$ ($J$ = 0, 1 and 2) to $^5L_6$, $^5D_3$, $^5D_2$ and $^5D_1$ were observed. For Eu-py2, slightly enhanced bands at around 330 nm were observed in the excitation spectra. These bands indicate that Eu-py2 shows photosensitized energy transfer from tmh ligands to Eu(III) center. The emission bands of Eu-py1 and Eu-py2 were observed at around 580, 590, 610, 650, and 700 nm, being attributed to the 4*f*–4*f* transitions of the Eu(III) ion ($^5D_0 \rightarrow {}^7F_{0-4}$). The spectral configuration and Stark splittings of Eu-py1 are much different from those of Eu-py2 for all observed transitions. The characteristic Stark splittings and spectral shapes of the transitions are attributed to each coordination geometry. For Eu-py1, relative strong $^5D_0 \rightarrow {}^7F_0$ emission was found, and the number of splittings for each transition are larger than the number for Eu-py2. This suggests stronger crystal fields in seven-coordinated structure, which is related to its asymmetry.

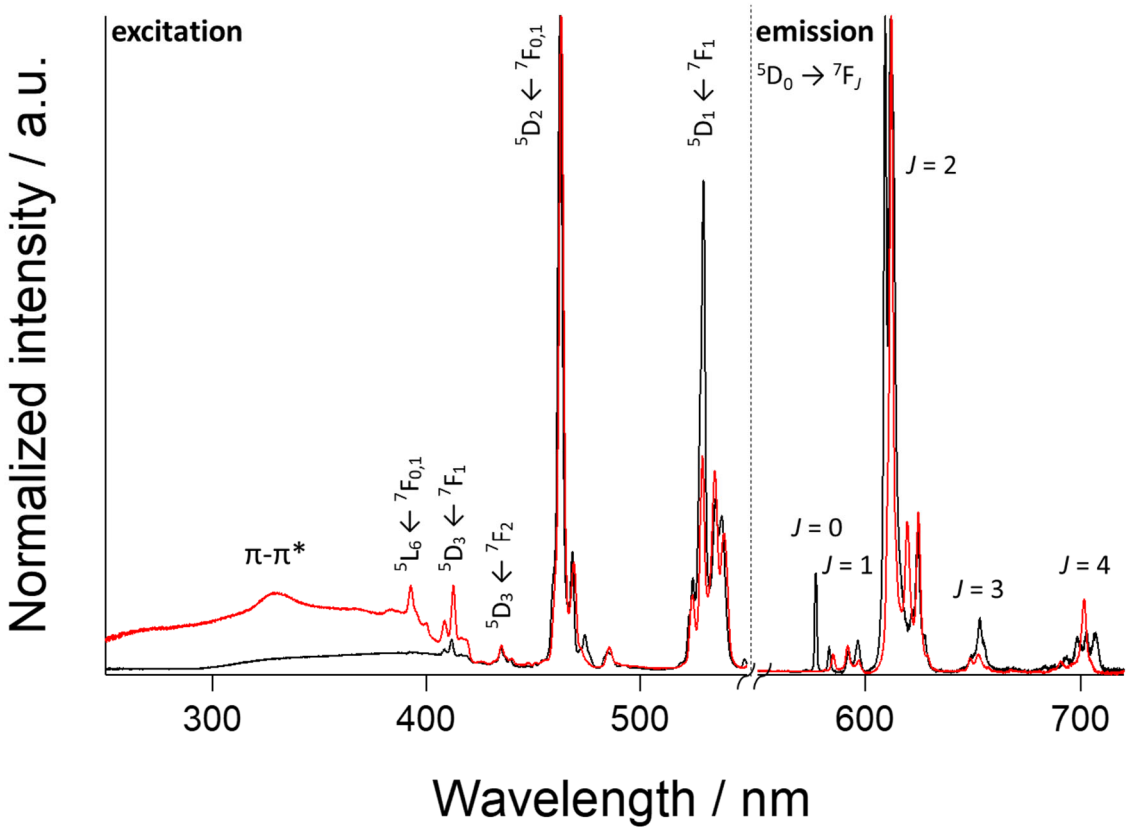


**Figure 4.** Excitation (left) and emission (right) spectra of Eu-py1 (black line) and Eu-py2 (red line) in solid state at room temperature. Excitation spectra were recorded with emission at 612 nm ($^5D_0 \rightarrow {}^7F_2$). Emission spectra were excited at 380 nm. Data normalized at their peak tops.

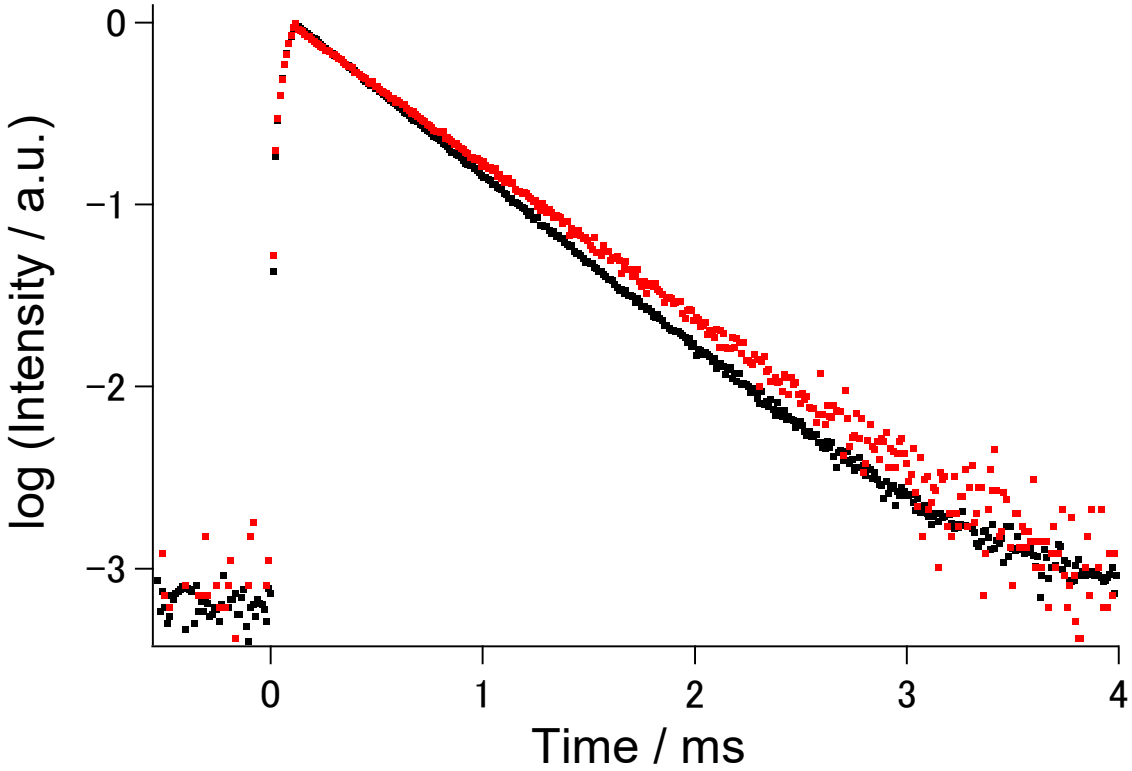


**Figure 5.** Emission decay profiles of Eu-py1 (black dots) and Eu-py2 (red dots) under 356 nm excitation at room temperature. Detection wavelength was set to 612 nm ($^5D_0 \rightarrow {}^7F_2$). The emission lifetimes were obtained from single-exponential analyses.

Emission lifetime (Figure 5), quantum yields and radiative/non-radiative rate constants for Eu-py1 and Eu-py2 were summarized in Table 1. In order to avoid the contribution of LMCT band, intrinsic quantum yields $\Phi_{ff}$ are measured using photo-irradiation at 530 nm ($^5D_1 \leftarrow {}^7F_1$). The measured $\Phi_{ff}$ values of Eu-py1 and Eu-py2 were found to be 60% and 63%, respectively (Check SI: Table S8 for detailed information). The $k_r$ value for Eu-py1 was slightly larger than that for Eu-py2.

**Table 1.** Photophysical properties of Eu-py1 and Eu-py2 under air atmosphere

| | Coordination structure | $T_{obs}$ / ms | $\Phi_{ff}$ [a] | $k_r$ / $s^{-1}$ | $k_{nr}$ / $s^{-1}$ |
|---|---|---|---|---|---|

| | | | | | |
|---|---|---|---|---|---|
| Eu-py1 | 7-MCO ($C_{3v}$) | 0.45 | 60 % | $1.33\times10^3$ | $8.89\times10^2$ |
| Eu-py2 | 8-SAP ($D_{4d}$) | 0.51 | 63 % | $1.26\times10^3$ | $7.06\times10^2$ |

a: Measured using integrating sphere ($\lambda_{ex}$ = 530 nm: $^5D_1 \leftarrow {}^7F_1$); $k_r = \Phi_{ff} \times T_{obs}^{-1}$; $k_{nr} = T_{obs}^{-1} - k_r$.

The emission quantum yields excited at predominant $\pi$-$\pi^*$ (330 nm) bands and predominant LMCT (400 nm) bands were measured under air and argon (absorption band assignment: Figure 3. Quantum yields results: Table 2). The $\Phi_{330}$ of Eu-py1 in air was similar to that of $\Phi_{330}$ in argon. From this result, the photosensitized energy transfer process of Eu-py1 is independent of the excited triplet state in tmh ligand. The energy transfer process of Eu-py2 is also not affected by the excited triplet state in tmh ligand ($\Phi_{330\_air}$ and $\Phi_{330\_Ar}$ for Eu-py2; $\Phi_{330\_air}$ and $\Phi_{330\_Ar}$ for Eu-py2 under pyridine solution: SI, Table S9). We found that $\Phi_{330\_air}$ and $\Phi_{330\_Ar}$ are similar to the $\Phi_{400\_air}$ and $\Phi_{400\_Ar}$. Therefore, the excited state of Eu(III) ion is achieved by the energy transfer of excited LMCT state under UV or blue light irradiation.

The average quantum yield $\Phi_{average}$ was calculated using the average quantum yield of $\Phi_{330\_air}$, $\Phi_{330\_Ar}$, $\Phi_{400\_air}$ and $\Phi_{400\_Ar}$ in Eu-py1 and Eu-py2. We calculated the photosensitized energy transfer efficiency $\eta_{sens}$ based on the $\Phi_{average}$ (Table 2) and intrinsic emission quantum yield $\Phi_{ff}$ (Table 1). The energy transfer efficiency $\eta_{sens}$ of Eu-py2 (3.3%) is eight times as large as that of Eu-py1 (0.4%). We conclude that the photosensitized energy transfer efficiency depends on the coordination geometry, related to the LMCT band.

**Table 2.** Quantum yields and energy transfer efficiency for Eu-py1 and Eu-py2 under different conditions

| | $\Phi_{330\_air}$[a] | $\Phi_{330\_Ar}$[a] | $\Phi_{400\_air}$[b] | $\Phi_{400\_Ar}$[b] | $\Phi_{average}$ | $\eta_{sens}$ |
|---|---|---|---|---|---|---|
| Eu-py1 | 0.24 ± 0.03 % | 0.21 ± 0.01 % | 0.31 ± 0.03 % | 0.27 ± 0.01 % | 0.26 % | 0.4 % |

| | | | | | | |
|---|---|---|---|---|---|---|
| Eu-py2 | 2.2 ± 0.2 % | 1.8 ± 0.03 % | 2.2 ± 0.1 % | 2.3 ± 0.3 % | 2.1 % | 3.3 % |

a: Measured using integrating sphere ($\lambda_{ex}$ = 330 nm); b: Measured using integrating sphere ($\lambda_{ex}$ = 400 nm). $\eta_{sens} = \Phi_{average} \times \Phi_{ff}^{-1}$.

## Theoretical calculations

In order to confirm the energy level and characteristics of LMCT bands in Eu-py1 and Eu-py2, theoretical calculations were performed. After geometry-optimization in the ground states by DFT (B3LYP-D3) (SI: Table S6 and Table S7), average Eu-$O_{tmh}$ distances for Eu-py1 and Eu-py2 were calculated to be 2.331 Å and 2.362 Å, respectively. Average Eu-N distances in pyridine ligands for Eu-py1 and Eu-py2 were also estimated to be 2.614 Å and 2.636 Å, respectively. Calculated distances in Eu-py2 were longer than those of Eu-py1, which are similar to the single-crystal data.

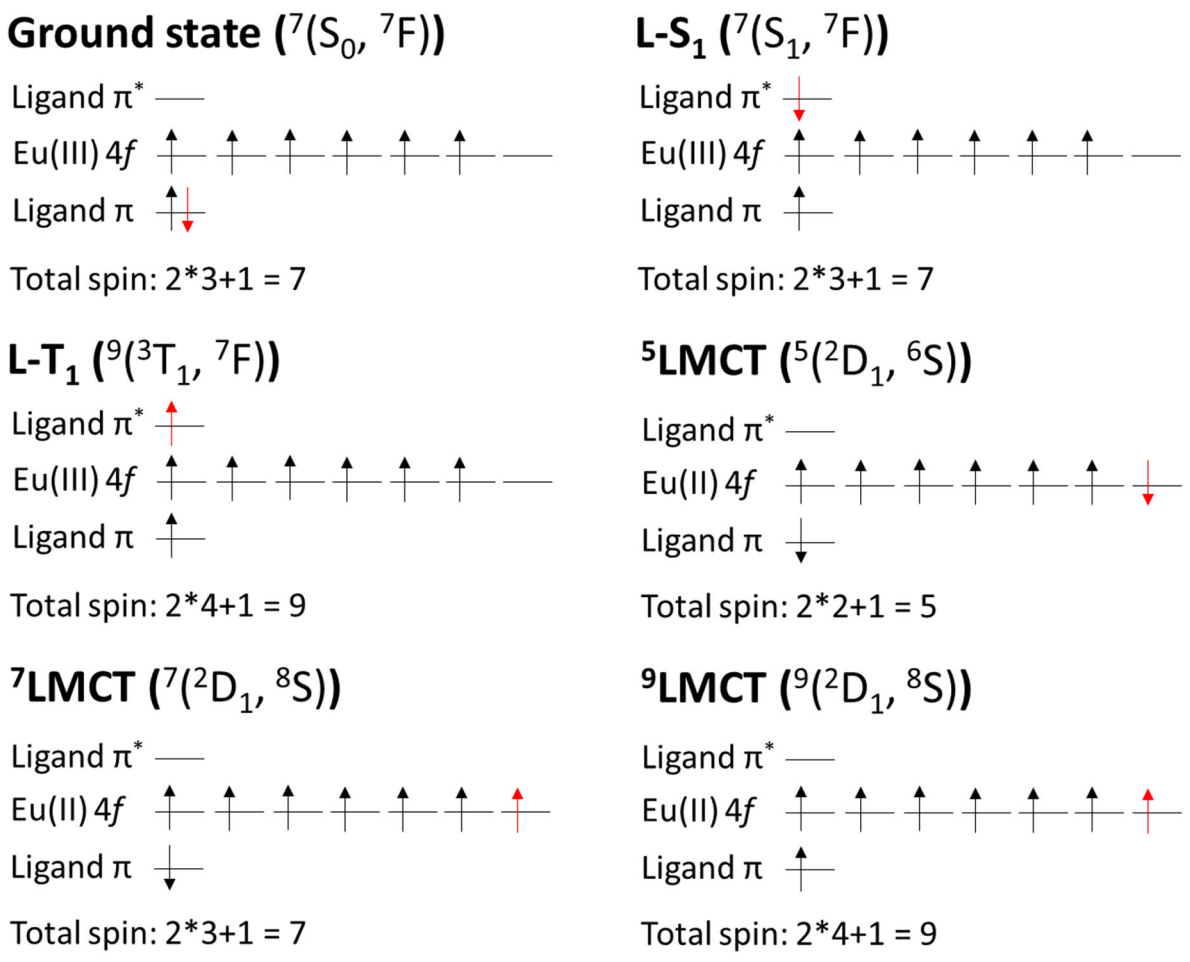


**Figure 6.** Illustration of open-shell configurations of ground, excited and LMCT states with their corresponding total spin multiplicity.

The open-shell configurations of LMCT states in Eu(III) complexes were illustrated in Figure 6. Based on the photophysical analyses, the photosensitized energy transfers of Eu-py1 and Eu-py2 occur from their LMCT states. The excited state calculations were focused on the spin-allowed (considering energy transfer from singlet state) transition to $^7$LMCT in Figure 6. The $^7$LMCT energy level for Eu-py1 (CN-7) was lower than that of Eu-py2 (CN-8) as shown in Table 3 and Table 4. The LMCT states by the quantum chemical calculation agree with the absorption reflectance spectra in Eu-py1 (CN-7) and Eu-py2 (CN-8). Spin-forbidden (considering energy transfer from singlet state) transitions to $^9$LMCT and $^5$LMCT were also calculated, although their absorptions were not observed from their intrinsic small oscillator

strengths. The $^{5}$LMCT/$^{9}$LMCT levels of Eu-py1 and Eu-py2 were found to be 49,035/23,476 cm$^{-1}$ and 49,936/24,239 cm$^{-1}$ (SI: Table S10), respectively.

**Table 3** - Excitation energies for $^{7}$LMCT states of Eu-py1 obtained by TD-DFT calculation

| Excitation energy / cm$^{-1}$ (wavelength / nm) | Oscillator strength | Main configuration |
|---|---|---|
| 24,356 (410.58) | 0.0057 | HOMO → LUMO |
| 24,401 (409.81) | 0.0007 | HOMO-1 → LUMO |
| 26,204 (381.62) | 0.0023 | HOMO-2 → LUMO |
| 27,438 (364.46) | 0.0047 | HOMO-3 → LUMO |
| 28,268 (353.76) | 0.0141 | HOMO-4 → LUMO |
| 29,075 (343.93) | 0.0057 | HOMO-5 → LUMO |

**Table 4** - Excitation energies for $^{7}$LMCT states of Eu-py2 obtained by TD-DFT calculation

| Excitation energy / cm$^{-1}$ (wavelength / nm) | Oscillator strength | Main configuration |
|---|---|---|
| 25,311 (395.08) | 0.0031 | HOMO → LUMO |
| 26,448 (378.11) | 0.0029 | HOMO-1 → LUMO |
| 27,288 (366.46) | 0.0032 | HOMO-2 → LUMO |
| 28,394 (352.19) | 0.0142 | HOMO-3 → LUMO |
| 29,332 (340.92) | 0.0074 | HOMO-4 → LUMO |
| 29,997 (333.38) | 0.0044 | HOMO-5 → LUMO |

The π-4*f* mixing percentages[1] in HOMO and LUMO were calculated (Table 5, SI: Tables S4-S5 and Figures S1-S2). Here, the structure was optimized with the B3LYP-D3 functional while the LC-BLYP functional, used in the excited-state calculations, was adopted for calculating MOs. The orbital mixing degree for Eu-py1 is slightly larger than that for Eu-py2, due to smaller average Eu-$O_{tmh}$ distances. The contribution percentage of π (tmh) in LUMO for Eu-py1 (4.2 %) is larger than that for Eu-py2 (3.9%). Therefore, larger π-4*f* orbital mixing in Eu-py1 leads to the lowering of LUMO (4*f*) level of Eu(III) complex (SI: Table S4-S5).[61] Such a π-4*f* orbital mixing in Eu-py1 promotes the decrease of HOMO-LUMO energy gap in LMCT band, which is in agreement with spectroscopic estimation based on the reflectance spectra.

**Table 5.** Atomic orbital contributions of 4*f* and π ligands in HOMO and LUMO of Eu-py1 and Eu-py2, corresponding to the lowest $^7$LMCT state

| | | 4*f* (Eu(III)) | π (tmh) | π (py) |
|---|---|---|---|---|
| Eu-py1 | HOMO | 0.6 % | 98.2 % | 0.1 % |
| | LUMO | 95.3 % | 4.2 % | 0.3 % |
| Eu-py2 | HOMO | 0.3 % | 98.3 % | 0.7 % |
| | LUMO | 95.7 % | 3.7 % | 0.4 % |

## Energy transfer analyses

From the photophysical and quantum chemical calculation results, we illustrated the photosensitized energy transfer processes for Eu-py1 and Eu-py2 in Figure 7. The ligand triplet

[1] The contribution of the 4*f* orbitals to the focusing MO (*p*) was evaluated as sum of the overlap integrals between AO $\mu$ and MO *p* over all *f* AOs in Eu, $\sum_{\mu \in f(\mathrm{Eu})} \langle \mu | p \rangle$ , while the contributions of the π(tmh)/π(py) were evaluated as sum of those over all AOs in tmh/py.

L-$T_1$ ($^9(T_1, {}^7F)$: Figure 6) energy level of Eu-py1 and Eu-py2 were estimated using phosphorescence spectra of isostructural Gd-py1 and Gd-py2, which are found to be approximately 25,000 $cm^{-1}$ for both complexes (SI: Figure S6). The photosensitized energy transfer processes are independent of excited triplet states of tmh ligand and $^5$LMCT/$^9$LMCT states, because the quantum yields are not affected by the presence of oxygen (Table 2 and SI: Table S8). Time-resolved emission decay profiles also indicated that the rate constant of $^5D_1 \rightarrow {}^5D_0$ transition is the same for Eu-py1 and Eu-py2 (SI: Figure S5). We consider that the $^5D_1$ level of Eu(III) is independent of LMCT-based quenching processes.

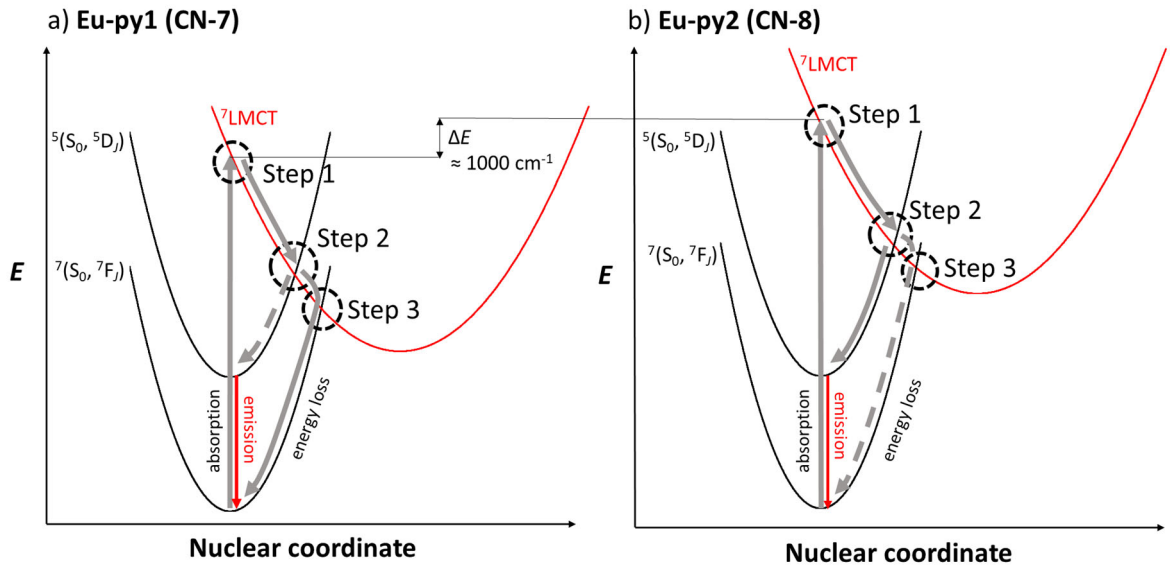


**Figure 7.** Proposed energy transfer mechanisms of a) Eu-py1 and b) Eu-py2 at room temperature under 400 nm light irradiation.

In Figure 7, formations of $^7$LMCT states for Eu-py1 and Eu-py2 are achieved by irradiation at 400 nm (step 1: LMCT direct excitation). Energy transfer from LMCT to excited state of Eu(III) occurs from cross-over in their respective potential curves (step 2: energy transfer from $^7$LMCT to $^5(S_0, {}^5D_J)$). Here, fast energy transfer (<100 ns) from $^7$LMCT to Eu(III) excited states $^5(S_0, {}^5D_1)$ is proposed according to the time-resolved emission decay profiles (SI: Figure S5). We also consider the possibility of the energy transfer from $^7$LMCT to higher Eu(III) excited

states, $^5(S_0, {}^5D_2)$ or $^5(S_0, {}^5D_3)$. The step 2 process dominates the photosensitized energy transfer efficiency. The energy transfer efficiency for Eu-py2 (3.3%) was higher than that for Eu-py1 (0.4%). In order to investigate these energy transfer processes, we measured the back energy transfer between $^5(S_0, {}^5D_0)$ and $^7$LMCT using temperature-depended emission lifetimes (SI: Figure S4 and Table S11).

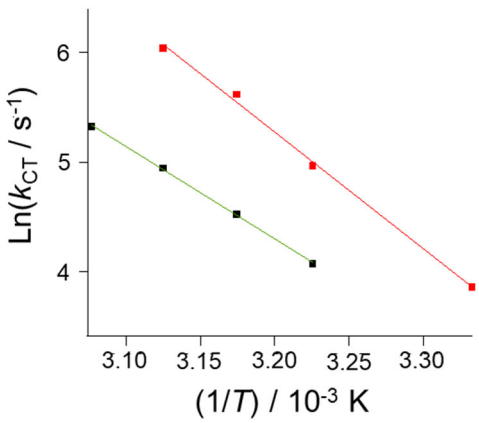


**Figure 8.** Arrhenius analyses of emission lifetime temperature dependence for Eu-py1 (black dot and green fitting line) and Eu-py2 (red dot and pink fitting line). Arrhenius equation: $\ln(k_{CT}) = \ln(A) - (E_a/k_B T)$. $k_B$ is the Boltzmann constant.

From their Arrhenius analyses (300-325 K), the frequency factors, $A$, of Eu-py1 and Eu-py2 were found to be $3.7 \times 10^{13}$ s$^{-1}$ and $7.2 \times 10^{15}$ s$^{-1}$, respectively (Figure 8). The $A$ value is affected by both the electronic coupling and the vibrational modes between 4*f*-4*f* excited electronic configuration and the $^7$LMCT state.[62,63] Because the electronic coupling in the Eu-py1 seems stronger than that in the Eu-py2 as estimated from the quantum chemical calculations, the frequency factor difference can only be explained by the effect from vibrational modes. We can conclude that small variations in the LMCT levels would cause substantial changes in the energy transfer efficiency. Finally, the molecule transitions from the LMCT to the ground state as a thermal relaxation (step 3). This thermal relaxation process causes an effective energy loss and promote the small $\Phi_{average}$ obtained for Eu-py1 and Eu-py2.

In summary, the excited molecule reaches the emitting level of Eu(III) ion ($^5D_0$) through LMCT states. The energy transfer processes in Eu-py1 and Eu-py2 are influenced by the energy level of these LMCT states and geometry/vibrational modification between LMCT and $^5D_J$ states.

## Conclusion

Two Eu(III) complexes, Eu-py1 with monocapped octahedron (CN-7, pseudo-$C_{3v}$ symmetry) and Eu-py2 with square antiprism (CN-8, pseudo-$D_{4d}$ symmetry) coordination environments, were synthesized. TD-DFT calculations and reflectance spectra indicated that the energy level of $^7$LMCT states for Eu-py1 (24,355 cm$^{-1}$) is different from that for Eu-py2 (25,311 cm$^{-1}$). The energy level difference in LMCT is dominated by Eu-$O_{ligand}$ distance and π-4*f* orbital mixing degree in Eu(III) complex. Eight-coordinated Eu(III) complex with longer Eu-$O_{ligand}$ distance shows lower degree of π-4*f* orbital mixing, which promotes LMCT states at higher energy level. According to the Arrhenius analyses, not only the electronic degree of freedom, but also the vibrational degree of freedom between $^7$LMCT and $^5D_J$ states for Eu-py2 impact the energy transfer. As a result, the higher $^7$LMCT energy level and geometry difference in Eu-py2 (CN-8) provide increase of the photosensitized energy transfer. Coordination geometry plays an important role for LMCT-controlled photosensitized Eu(III) complex. We are currently working on external stimulated crystal structure control in lanthanide complex. We hope to open new possibilities of coordination geometry control and photophysical properties for lanthanide complex.

Significant control on LMCT state through coordination structural change can also improve the luminescence efficiency of Eu(III) complexes for optical applications, such as display devices, thermal-sensing paints and biomedical sensors. Further geometrical-control on LMCT state and energy transfer processes in Eu(III) complexes can expand their use for frontier 4*f* photophysics.

## Associated Content

**Supporting Information**: Schematic reaction of pyridine-based $Ln(tmh)_3$ complexes; Crystallographic data; Calculated SHAPE values for Eu(III) ions in Eu-py1 and Eu-py2; Atomic orbital contributions for the MOs responsible for $^7$LMCT states of Eu-py1 and Eu-py2; Cartesian coordinates of Eu-py1 and Eu-py2 for optimized structure obtained from DFT calculations; MOs responsible for $^7$LMCT states of Eu-py1 and Eu-py2; Reflectance spectra of Ln-py1 and Ln-py2; Emission quantum yields for Eu-py1 and Eu-py2 under different conditions; Emission quantum yields for Eu-py2 under pyridine solution ($10^{-4}$ M); Excitation energies for $^5$LMCT and $^9$LMCT states of Eu-py1 and Eu-py2 obtained by TD-DFT calculation; Emission lifetime temperature dependence derived from $^5D_0 \rightarrow {}^7F_J$ for Eu-py1 and Eu-py2; Arrhenius analyses (Frequency factor $A$ and activation energy $E_a$ calculation) and equation for emission lifetime temperature dependence of Eu-py1 and Eu-py2; Time-resolved emission decay profiles derived from $^5D_0$ and $^5D_1$ states for Eu-py1 and Eu-py2; Phosphorescence spectra of Gd-py1 and Gd-py2.

**CIF files** for Eu-py1, Eu-py2, Gd-py1 and Gd-py2.

## Author Information

**Corresponding Author**

*Tel.: +81 11 706 7114. Fax: +81 11 706 7114. E-mail: hasegaway@eng.hokudai.ac.jp.

**Author Contributions**

The manuscript was written through contributions of all authors. All authors have given approval to the final version of the manuscript.

## Acknowledgment

This work was supported by JSPS KAKENHI Grant Number JP18H02041, 20H04653, 20H05197, 20K21201, 19H04556 and 20H02748 of the Ministry of Education, Culture, Sports,

Science and Technology (MEXT) of Japan. This work was also supported by the Institute for Chemical Reaction Design and Discovery (ICReDD), established by the World Premier International Research Initiative (WPI) and JSPS Research Fellow (no. 19J20713) of MEXT, Japan. The authors express sincere thanks to Prof. H. Ito and Dr. T. Seki of Hokkaido University for measurements of single crystal X-ray diffractions.

## Abbreviations

tmh, trimethylheptandionate; py, pyridine; LMCT, ligand-to-metal charge transfer; Eu, europium; Gd, gadolinium; Ln, lanthanide; nm, nanometer.

## References

(1) Gil-Rostra, J.; Ferrer, F. J.; Espinós, J. P.; González-Elipe, A. R.; Yubero, F. Energy-Sensitive Ion- and Cathode-Luminescent Radiation-Beam Monitors Based on Multilayer Thin-Film Designs. *CS Appl. Mater. Interfaces* **2017**, *9* (19), 16313–16320.

(2) Rangari, V. v.; Dhoble, S. J. Synthesis and Photoluminescence Studies of Ba(Gd, Ln)B9O16:Eu3+(Ln=La,Y) Phosphors for n-UV LED Lighting and Display Devices. *J. Rare Earths* **2015**, *33* (2), 140–147.

(3) Du, P.; Krishna Bharat, L.; Yu, J. S. Strong Red Emission in Eu3+/Bi3+ions Codoped CaWO4phosphors for White Light-Emitting Diode and Field-Emission Display Applications. *J. Alloys Compd.* **2015**, *633*, 37–41.

(4) Hou, D.; Chen, W.; Ding, X.; Liang, H.; Zheng, L.; Zhang, J. Intense Blue Emission Phosphor BaCa2MgSi2O8: Eu2+ for Fluorescent Lamps. *ECS J. Solid State Sci. Technol.* **2013**, *2* (4), R79–R81.

(5) Xu, H.; Wang, J.; Wei, Y.; Xie, G.; Xue, Q.; Deng, Z.; Huang, W. A Unique White Electroluminescent One-Dimensional Europium(iii) Coordination Polymer. *J. Mater. Chem. C* **2015**, *3* (9), 1893–1903.

(6) Xu, H.; Yin, K.; Huang, W. Highly Improved Electroluminescence from a Series of Novel Eu111complexes with Functional Single-Coordinate Phosphine Oxide Ligands: Tuning the Intramolecular Energy Transfer, Morphology, and Carrier Injection Ability of the Complexes. *Chem. - Eur. J.* **2007**, *13* (36), 10281–10293.

(7) Ling, Q.; Song, Y.; Ding, S. J.; Zhu, C.; Chan, D. S. H.; Kwong, D. L.; Kang, E. T.; Neoh, K. G. Non-Volatile Polymer Memory Device Based on a Novel Copolymer of N-Vinylcarbazole and Eu-Complexed Vinylbenzoate. *Adv. Mater.* **2005**, *17* (4), 455–459.

(8) Li, X. L.; Chen, C. L.; Xiao, H. P.; Wang, A. L.; Liu, C. M.; Zheng, X.; Gao, L. J.; Yang, X. G.; Fang, S. M. Luminescent, Magnetic and Ferroelectric Properties of Noncentrosymmetric Chain-like Complexes Composed of Nine-Coordinate Lanthanide Ions. *Dalton Trans.* **2013**, *42* (43), 15317–15325.

(9) Yang, D.; Xu, Y.; Yao, Y.; Zhang, J.; Wang, J.; Wang, Y. A Red Light-Emitting Ionic Europium (III) Complex Applied in near UV LED. *Synth. Met.* **2016**, *221*, 236–241.

(10) Reichardt, C.; Schneider, K. R. A.; Sainuddin, T.; Wächtler, M.; McFarland, S. A.; Dietzek, B. Excited State Dynamics of a Photobiologically Active Ru(II) Dyad Are Altered in Biologically Relevant Environments. *J. Phys Chem. A* **2017**, *121* (30), 5635–5644.

(11) Szaciłowski, K.; Macyk, W.; Drzewiecka-Matuszek, A.; Brindell, M.; Stochel, G. Bioinorganic Photochemistry: Frontiers and Mechanisms. *Chem. Rev.* **2005**, *105* (6), 2647–2694.

(12) Martínez, M.; Carranza, M. P.; Massaguer, A.; Santos, L.; Organero, J. A.; Aliende, C.; de Llorens, R.; Ng-Choi, I.; Feliu, L.; Planas, M.; et al. Synthesis and Biological Evaluation of Ru(II) and Pt(II) Complexes Bearing Carboxyl Groups as Potential Anticancer Targeted Drugs. *Inorg. Chem.* **2017**, *56* (22), 13679–13696.

(13) Muller, G. Luminescent Chiral Lanthanide(Iii) Complexes as Potential Molecular Probes. *Dalton Trans.* **2009**, *0* (44), 9692–9707.

(14) Jia, J.; Zhang, Y.; Zheng, M.; Shan, C.; Yan, H.; Wu, W.; Gao, X.; Cheng, B.; Liu, W.; Tang, Y. Functionalized Eu(III)-Based Nanoscale Metal-Organic Framework to Achieve Near-IR-Triggered and -Targeted Two-Photon Absorption Photodynamic Therapy. *Inorg. Chem.* **2018**, *57* (1), 300–310.

(15) Heffern, M. C.; Matosziuk, L. M.; Meade, T. J. Lanthanide Probes for Bioresponsive Imaging. *Chem. Rev.* **2014**, *114* (8), 4496–4539.

(16) Lever, A. B. P. *Inorganic Electronic Spectroscopy*; Elsevier: Amsterdam, The Netherlands, 1968.

(17) Komuro, T.; Furuyama, K.; Kitano, T.; Tobita, H. Synthesis of a 14-Electron Iridium(III) Complex with a Xanthene-Based Bis(Silyl) Chelate Ligand (Xantsil): A Distorted Seesaw-Shaped Fourcoordinate Geometry and Reactions Leading to 16-Electron Complexes. *J. Organomet. Chem.* **2014**, *751*, 686–694.

(18) DeArmond, M. K.; Hillis, J. E. Luminescence of Transition Metal D6 Chelates. *The J. Chem. Phys.* **1971**, *54* (5), 2247–2253.

(19) Chábera, P.; Liu, Y.; Prakash, O.; Thyrhaug, E.; Nahhas, A. el; Honarfar, A.; Essén, S.; Fredin, L. A.; Harlang, T. C. B.; Kjær, K. S.; et al. A Low-Spin Fe(III) Complex with 100-Ps Ligand-to-Metal Charge Transfer Photoluminescence. *Nature* **2017**, *543* (7647), 695–699.

(20) de Bettencourt-Dias, A. Lanthanide-Based Emitting Materials in Light-Emitting Diodes. *Dalton Trans.* **2007**, *0* (22), 2229–2241.

(21) Bünzli, J. C. G. On the Design of Highly Luminescent Lanthanide Complexes. *Coord. Chem. Rev.* **2015**, *293–294*, 19–47.

(22) Judd, B. R. Optical Absorption Intensities of Rare-Earth Ions. *Phys. Rev.* **1962**, *127* (3), 750–761.

(23) Ofelt, G. S. Intensities of Crystal Spectra of Rare-Earth Ions. *J. Chem. Phys.* **1962**, *37* (3), 511–520.

(24) D'Aléo, A.; Picot, A.; Beeby, A.; Williams, J. A. G.; le Guennic, B.; Andraud, C.; Maury, O. Efficient Sensitization of Europium, Ytterbium, and Neodymium Functionalized Tris-Dipicolinate Lanthanide Complexes through Tunable Charge-Transfer Excited States. *Inorg. Chem.* **2008**, *47* (22), 10258–10268.

(25) Napier, G. D. R.; Neilson, J. D.; Shepherd, T. M. Charge-Transfer Excited State in Tris(Acetylacetonato) Europium(III). *Chem. Phys. Lett* **1975**, *31* (2), 328–330.

(26) Berry, M. T.; Stanley May, P.; Xu, H. Temperature Dependence of the Eu 3+5 D 0 Lifetime in Europium Tris(2,2,6,6-Tetramethyl-3,5-Heptanedionato). *J. Phys. Chem.* **1996**, *100* (22), 9216–9222.

(27) An, Y.; Schramm, G. E.; Berry, M. T. Ligand-to-Metal Charge-Transfer Quenching of the Eu3+(5D1) State in Europium-Doped Tris(2,2,6,6-Tetramethyl-3,5-Heptanedionato)Gadolinium (III). *J. Lumin.* **2002**, *97* (1), 7–12.

(28) Miranda, Y. C.; Pereira, L. L. A. L.; Barbosa, J. H. P.; Brito, H. F.; Felinto, M. C. F. C.; Malta, O. L.; Faustino, W. M.; Teotonio, E. E. S. The Role of the Ligand-to-Metal Charge-Transfer State in the Dipivaloylmethanate-Lanthanide Intramolecular Energy Transfer Process. *Eur. J. Inorg. Chem.* **2015**, *2015* (18), 3019–3027.

(29) Borges, A. S.; Fulgêncio, F.; da Silva, J. G.; Ribeiro-Santos, T. A.; Diniz, R.; Windmöller, D.; Magalhães, W. F.; Araujo, M. H. Luminescence and Positron Spectroscopies Studies of Tris(2,2,6,6-Tetramethyl-3,5-Heptanedionate) Europium(III) and Terbium(III) Complexes Containing 2-Pyrrolidone as Coligand. *J. Lumin.* **2019**, *205*, 72–81.

(30) Kitagawa, Y.; Kumagai, M.; Ferreira da Rosa, P. P.; Fushimi, K.; Hasegawa, Y. Long-range LMCT Coupling in Eu(III) Coordination Polymers for an Effective Molecular Luminescent Thermometer. *Chem. - Eur. J.* **2020**. https://doi.org/10.1002/chem.202003722

(31) Kitagawa, Y.; Kumagai, M.; Ferreira Da Rosa, P. P.; Fushimi, K.; Hasegawa, Y. First Demonstration of the π-f Orbital Interaction Depending on the Coordination Geometry in Eu(Iii) Luminophores. *Dalton Trans.* **2020**, *49* (10), 3098–3101.

(32) Faustino, W. M.; Malta, O. L.; Teotonio, E. E. S.; Brito, H. F.; Simas, A. M.; de Sa, G. F. Photoluminescence of Europium(III) Dithiocarbamate Complexes: Electronic Structure, Charge Transfer and Energy Transfer. *J. Phys. Chem. A* **2006**, *110* (7), 2510–2516.

(33) Faustino, W. M.; Malta, O. L.; Teotonio, E. E. S.; Brito, H. F.; Simas, A. M.; de Sá, G. F. Photoluminescence of Europium(III) Dithiocarbamate Complexes: Electronic Structure, Charge Transfer and Energy Transfer. *J. Phys. Chem. A* **2006**, *110* (7), 2510–2516.

(34) Faustino, W. M.; Malta, O. L.; de Sá, G. F. Intramolecular Energy Transfer through Charge Transfer State in Lanthanide Compounds: A Theoretical Approach. *J. Chem. Phys.* **2005**, *122* (5).

(35) Villata, L. S.; Wolcan, E.; Féliz, M. R.; Capparelli, A. L. Competition between Intraligand Triplet Excited State and LMCT on the Thermal Quenching in β-Diketonate Complexes of Europium(III). *J. Phys. Chem. A* **1999**, *103* (29), 5661–5666.

(36) Yanagisawa, K.; Kitagawa, Y.; Nakanishi, T.; Seki, T.; Fushimi, K.; Ito, H.; Hasegawa, Y. A Luminescent Dinuclear EuIII/TbIIIComplex with LMCT Band as a Single-Molecular Thermosensor. *Chem. - Eur. J.* **2018**, *24* (8), 1956–1961.

(37) Simonnet, M.; Suzuki, S.; Miyazaki, Y.; Kobayashi, T.; Yokoyama, K.; Yaita, T. Lanthanide Intra-Series Separation by a 1,10-Phenanthroline Derivative: Counterion Effect. *Solvent Extr. Ion Exch.* **2020**, *38* (4), 430–440.

(38) Yanagisawa, K.; Kitagawa, Y.; Nakanishi, T.; Akama, T.; Kobayashi, M.; Seki, T.; Fushimi, K.; Ito, H.; Taketsugu, T.; Hasegawa, Y. Enhanced Luminescence of Asymmetrical Seven-Coordinate EuIII Complexes Including LMCT Perturbation. *Eur. J. Inorg. Chem.* **2017**, *2017* (32), 3843–3848.

(39) Fulgêncio, F.; de Oliveira, F. C.; Ivashita, F. F.; Paesano, A.; Windmöller, D.; Marques-Netto, A.; Magalhães, W. F.; MacHado, J. C. Solid Eu(III) Complexes Studied by Positron Annihilation, Optical and Mössbauer Spectroscopies: Insights on the Positronium Formation Mechanism. *Spectrochim. Acta, Part A* **2012**, *92*, 415–418.

(40) Selbin, J.; Ahmad, N.; Bhacca, N. Preparation and Properties of Lanthanide Chelate Complexes. *Inorg. Chem.* **1971**, *10* (7), 1383–1387.

(41) Catton, G. A.; F. Alan, H.; Moss, G. P. Studies of the Conformations of the N.m.r. Shift Reagent Tris(2,2,6,6- Tetramethylheptane-3,5-Dionato)Europium(III) and Its Adducts by Means of Fluorescence Spectra. *J. Am. Chem. Soc.* **1972**, *94*, 1742.

(42) Spencer, R. D.; Weber, G. Influence of Brownian Rotations and Energy Transfer upon the Measurements of Fluorescence Lifetime. *J. Chem. Phys.* **1970**, *52* (4), 1654–1663.

(43) Sheldrick, G. M. A Short History of SHELX. *Acta Crystallogr., Sect. A: Found. Crystallogr.* **2008**, *64* (1), 112–122.

(44) Dolomanov, O. v.; Bourhis, L. J.; Gildea, R. J.; Howard, J. A. K.; Puschmann, H. OLEX2: A Complete Structure Solution, Refinement and Analysis Program. *J. Appl. Crystallogr.* **2009**, *42* (2), 339–341.

(45) Frisch MJ, Trucks GW, Schlegel HB, Scuseria GE, Robb M, Cheeseman JR, Scalmani G, Barone V, Mennucci B, Petersson GA, Nakatsuji H et al. *Gaussian 16, Revision A.03.* **2016**, p Gaussian, Inc., Wallingford CT.

(46) Becke, A. D. Density-Functional Thermochemistry . III . The Role of Exact Exchange. *J. Chem. Phys.* **1993**, *98*, 5648–5652.

(47) Stephens, P. J.; Devlin, F. J.; Chabalowski, C. F.; Frisch, M. J. Ab Initio Calculation of Vibrational Absorption and Circular Dichroism Spectra Using Density Functional Force Fields. *J. Phys. Chem.* **1994**, *98* (45), 11623–11627.

(48) Grimme, S.; Antony, J.; Ehrlich, S.; Krieg, H. A Consistent and Accurate Ab Initio Parametrization of Density Functional Dispersion Correction (DFT-D) for the 94 Elements H-Pu Cite. *J. Chem. Phys.* **2010**, *132*, 154104.

(49) Becke, A. D. Density-Functional Exchange-Energy Approximation with Correct Asymptotic Behavior. *Physical Review A* **1988**, *38*, 3098–3100.

(50) Lee, C.; Yang, W.; Parr, R. G. Development of the Colle-Salvetti Correlation-Energy Formula into a Functional of the Electron Density. *Phys. Rev. B* **1988**, *37*, 785–789.

(51) Tawada, Y.; Tsuneda, T.; Yanagisawa, S.; Yanai, T.; Hirao, K. A Long-Range-Corrected Time-Dependent Density Functional Theory. *J. Chem. Phys.* **2004**, *120* (18), 8425–8433.

(52) Dunning, T. H. Gaussian Basis Sets for Use in Correlated Molecular Calculations. I. The Atoms Boron through Neon and Hydrogen. *J. Chem. Phys.* **1989**, *90* (2), 1007–1023.

(53) Dolg, M.; Stoll, H.; Savin, A.; Preuss, H. Energy-Adjusted Pseudopotentials for the Rare Earth Elements. *Theor. Chim. Acta* **1989**, *75* (3), 173–194.

(54) Cramer, R. E.; Seff, K. Crystal and Molecular Structure of a Nuclear Magnetic Resonance Shift Reagent, the Dipyridine Adduct of Tris-[(2,2,6,6-Tetramethylheptane-3,5-Dionato) Europium(III), Eu(Dpm)3(Py)2]. *J. Chem. Soc., Chem. Commun.* **1972**, *0* (7), 400–401.

(55) Brown, T. D.; Shepherd, T. M. Anomalous Triplet-State Behaviour in Solid Tris(Dipivaloylmethanato)Terbium(III). *J. Chem. Soc., Dalton Trans.* **1972**, No. 15, 1616–1619.

(56) Casanova, D.; Llunell, M.; Alemany, P.; Alvarez, S. The Rich Stereochemistry of Eight-Vertex Polyhedra: A Continuous Shape Measures Study. *Chem. - Eur J.* **2005**, *11* (5), 1479–1494.

(57) Pinsky, M.; Avnir, D. Continuous Symmetry Measures. 5. The Classical Polyhedra. *Inorg. Chem.* **1998**, *37* (3), 5575–5582.

(58) Universitat de Barcelona. Electronic Structure Group - SHAPE 2.1 http://www.ee.ub.edu/index.php?option=com_content&view=article&id=575:shape-available&catid=80:news&Itemid=466 (accessed Feb 21, 2018).

(59) Fernandes, J. A.; Sá Ferreira, R. A.; Pillinger, M.; Carlos, L. D.; Gonçalves, I. S.; Ribeiro-Claro, P. J. A. Spectroscopic Studies of Europium(III) and Gadolinium(III) Tris-β-Diketonate Complexes with Diazabutadiene Ligands. *Eur. J. Inorg. Chem.* **2004**, No. 19, 3913–3919.

(60) Görller-Walrand, C.; Fluyt, L.; Ceulemans, A.; Carnall, W. T. Magnetic Dipole Transitions as Standards for Judd – Ofelt Parametrization in Lanthanide Spectra. *J. Chem. Phys.* **1991**, *95*, 3099.

In general, emission spectra of Eu(III) complexes are normalized at the spectral area of the magnetic-dipole transitions ($^5D_0 \rightarrow {}^7F_1$). This is usually done in the premise that the magnetic-dipole transition is not depended on outside factors, such as coordination environment. However, as show before, orbital mixing between Eu(III) 4*f* and tmh's π orbitals induces partial characterization of forced electric-dipole transition into the magnetic-dipole transition ($^5D_0 \rightarrow {}^7F_1$).

(61) Petoud, S.; Bünzli, J. C. G.; Glanzman, T.; Piguet, C.; Xiang, Q.; Thummel, R. P. Influence of Charge-Transfer States on the Eu(III) Luminescence in Mononuclear Triple Helical Complexes with Tridentate Aromatic Ligands. *J. Lumin.* **1999**, *82* (1), 69–79.

(62) Barigelletti, F.; Juris, A.; Balzani, V.; Belser, P.; von Zelewsky, A. Temperature Dependence of the Ru(Bpy)2(CN)2 and Ru(Bpy)2(i-Biq)2+ Luminescence. *J. Phys. Chem.* **1987**, *91* (5), 1095–1098.

(63) Abrahamsson, M. *Tuning of the Excited State Properties of Ruthenium (II) - Polypyridyl Complexes*; 2006.

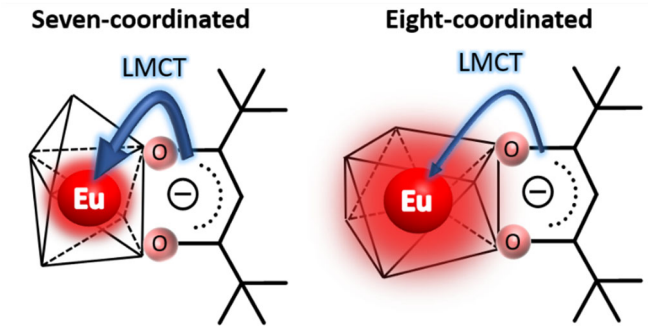


TOC Graphic